DOI: 10.13009/EUCASS2022-7236
9TH EUROPEAN CONFERENCE FOR AERONAUTICS AND SPACE SCIENCES (EUCASS)

Numerical simulations of lateral jet and supersonic crossflow interaction with various approaches

Efe Can Dağlı and Tezcan Ünlü***
**Roketsan Missiles Inc.*
Kemalpaşa Mahallesi Şehit Yüzbaşı Adem Kutlu Sokak No:21 06780 Elmadağ-Ankara-Türkiye
***Roketsan Missiles Inc.*
Kemalpaşa Mahallesi Şehit Yüzbaşı Adem Kutlu Sokak No:21 06780 Elmadağ-Ankara-Türkiye

Abstract
The numerical simulation methods investigation and validation on lateral jet systems which are effective at low dynamic pressures unlike the conventional control systems are carried out. First of the validation studies is focused on air spouting lateral jets. And other studies present jets which are operating with combustion products excluding and including the effect of reactions, respectively. Surface pressure and Mach number distributions are taken into consideration for numerical results. With the investigation studies, numerical simulation methods for jet and crossflow interactions which are air-air, air-exhaust gases excluding reactions and air-exhaust gases including reactions are determined and validated.

1. Introduction

A missile relies on many engineering disciplines such as electronics, propulsion, aerodynamics, mechanical design, etc. These disciplines are working in harmony to be able to build a precise missile. In this study, the focus is on external aerodynamics and manoeuvre capability. The conventional method for missile manoeuvrability is aerodynamic surfaces (canards, wings, and tails) which have a major disadvantage of losing effectiveness at low velocity and high elevation. To cope with this problem, reaction attitude control systems are developed. With the use of these systems, more agile and more precise munitions are possible. These control systems consist of thrust vector control (TVC) and lateral jet control. TVC is based on changing the direction of the rocket thrust vector and obtaining a moment on the missile body. TVC has been used in the industry widely depending on the complexity of the system, but it has some drawbacks. The method increases the missile weight since it uses flow-distorting vanes at the engine exit. Moreover, the method causes a blockage at the engine exit, therefore the range of the missile decreases.

The next control system is lateral jet control which is the subject of this study. Lateral jet which is a manoeuvering technique can be defined as ejecting the high pressure, high velocity gases into the free-stream flow and generating thrust in desired direction. While the lateral jet system increasing the manoeuvrability of the missile, it causes a very complex flow domain. The effect of this complex flow domain on missile aerodynamic performance should be checked in the earlier design phases of the missile using the validated tools.

In this study, numerical simulation methods containing various approaches will be validated using the experimental data from the literature. Validation in this study has three aspects of view for the lateral jet. In the first section, air spouting lateral jet on a generic supersonic missile model is examined. In the second section, the jet spouts the combustion products of propellant. Nevertheless, secondary combustion of the products is not modelled in this section. In the last section, combustion products are modelled including the effect of secondary combustion. Numerical simulations are evaluated using the surface pressure data with the available numerical/experimental results from literature for the mentioned study cases. Lastly, several deductions are made for the accuracy of the numerical simulation approaches.

2. Lateral jet operating with air

As a first step for the validation studies, lateral jet operating with air is investigated. In this part, the effect of reactions and gas species is not taken into consideration, only the interactions between two flows are investigated.

DOI: 10.13009/EUCASS2022-7236

2.1 Test case details

Geometric details of the test model are presented in the Figure 1 [1]. Diameter of the model (D) is 40 mm and model consists of 2.8D length nose, 3.2D length cylindrical mid-body and 3D length flare aft-body. Diameter of the model base is 1.66D. Jet exit is located at the 4.3D axial distance from the nose tip and diameter of the exit is 0.1D. Also the jet exit is located on the 180° circumferential position. Moreover, three sets of pressure taps exist on the model body which is located on 180°, 150° and 120° circumferential positions. These pressure tap sets are presented as lines on the Figure 1. Surface pressure data obtained from these taps is used for validating CFD solution which is obtained using Fluent.

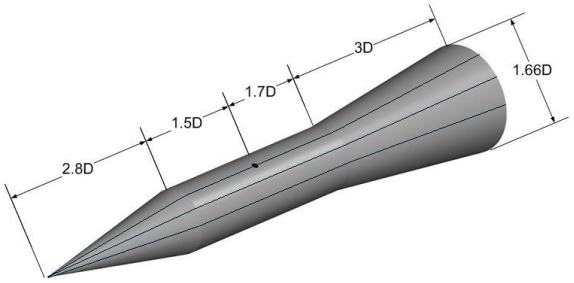

Figure 1: Geometrical properties of test model

Flow properties of the experiment are presented in Table 1 and it is stated that crossflow is air [1]. Pressure ratio (PR) is the ratio of the jet flow total pressure to the static pressure of the crossflow which is defined as the jet strength in the literature. In the reference, temperature and species of the jet flow is not clearly emphasized [1]. Therefore, static temperature of the jet flow is assumed to be equal to the crossflow temperature. Also, jet flow is assumed as air. In the calculation of the jet flow properties, ideal gas assumption is made and isentropic flow equations are used.

Table 1: Flow properties

Crossflow	**Jet Flow**
M = 2.8	M = 1
P_∞ [Pa] = 20793.2	PR - ($P_{0,j}$ / P_∞) = 100
T_∞ [K] = 108.96	

2.2 CFD methodology

For grid generation, software named Gambit and Tgrid are used. For the numerical simulation Ansys Fluent is used. For the jet boundary condition, mass flow inlet and for the crossflow pressure far field boundary types from Fluent are used. In the numerical simulation k-ε Realizable turbulence model is used. Generated volume grid is presented in Figure 2. In the generation of boundary layer grid y+~1 is accomplished for most of the domain. Volume grid consists of 4.6 million cells. More detail on the turbulence model selection and grid independency can be reached from previous studies [2], [3].

DOI: 10.13009/EUCASS2022-7236

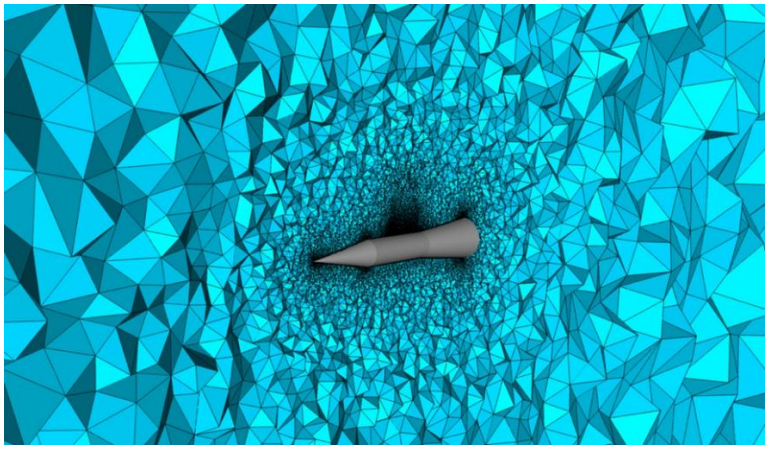

Figure 2: Generated volume grid

2.3 Results and discussion

In this section, numerical simulation results which are obtained with Fluent are presented. Pressure coefficient results for 180°, 150° and 120° circumferential positions on the model are presented and compared with experimental data in Figure 3, 4 and 5.

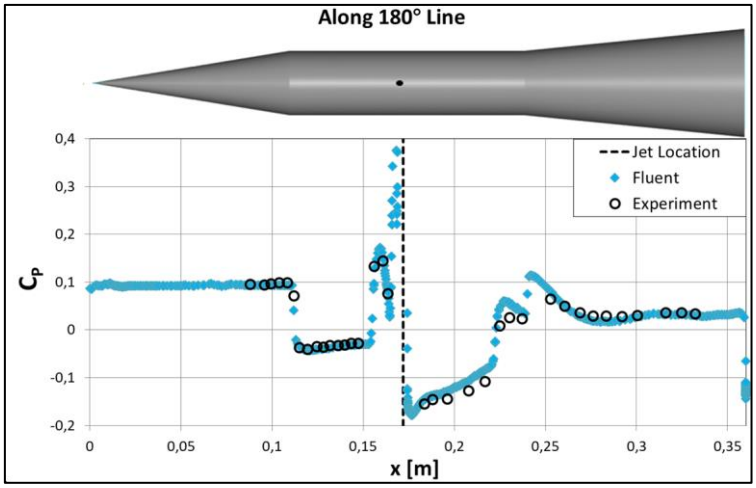

Figure 3: Pressure coefficient results for 180° circumferential position

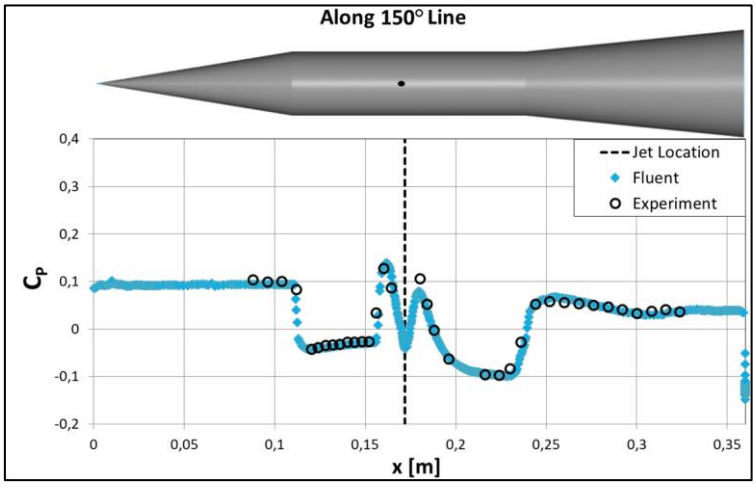

Figure 4: Pressure coefficient results for 150° circumferential position

DOI: 10.13009/EUCASS2022-7236

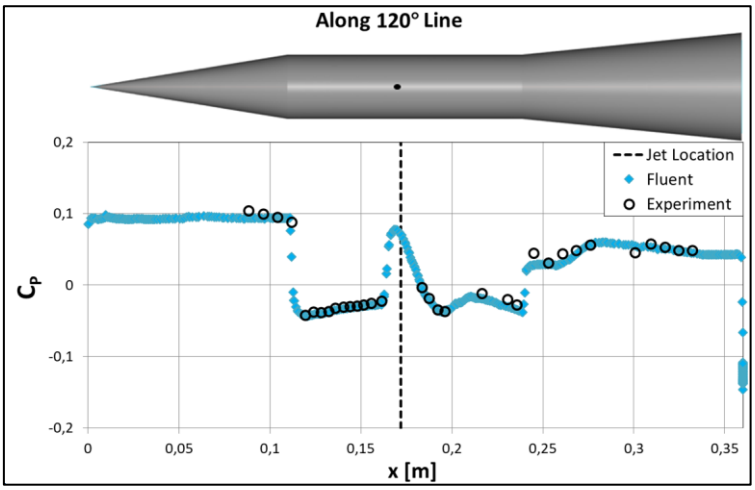

Figure 5: Pressure coefficient results for 120° circumferential position

From the Figure 3, 4 and 5, one can say that numerical simulation results are largely consistent with the experimental data except for small discrepancies. At the location x < 0.15 m where jet flow is not expected to affect flow, numerical simulation results and experimental data are well-matched for three different circumferential angles. Between 0.15 m < x < 0.17 m where jet flow causes abrupt pressure increase, results are in good agreement for three circumferential positions. At the location 0.17 m < x < 0.22 m, where recirculation occurs in the wake of the jet flow obstacle, results show similar characteristics. For the location 0.22 m < x < 0.24 m and 180° circumferential location results have some differences. At the mentioned region reattachment shock occurs. As a final evaluation, numerical simulation method solves the flow interactions sufficiently.

Distribution of the flow features are generated by post-processing the numerical solution and presented below for further examination of the flow domain. Pressure distribution around the missile is presented in the Figure 6. In the figure, nose shock which is shown with “1” is caused by the interaction of the nose of the model and the supersonic crossflow. Jet bow shock which is shown with “2” occurs due to the interaction of the crossflow and jet flow which are normal to each other. At point “3”, separation occurs due to adverse pressure gradient in the crossflow direction. At point “4”, there exists wake region occurring due to the jet flow obstacle.

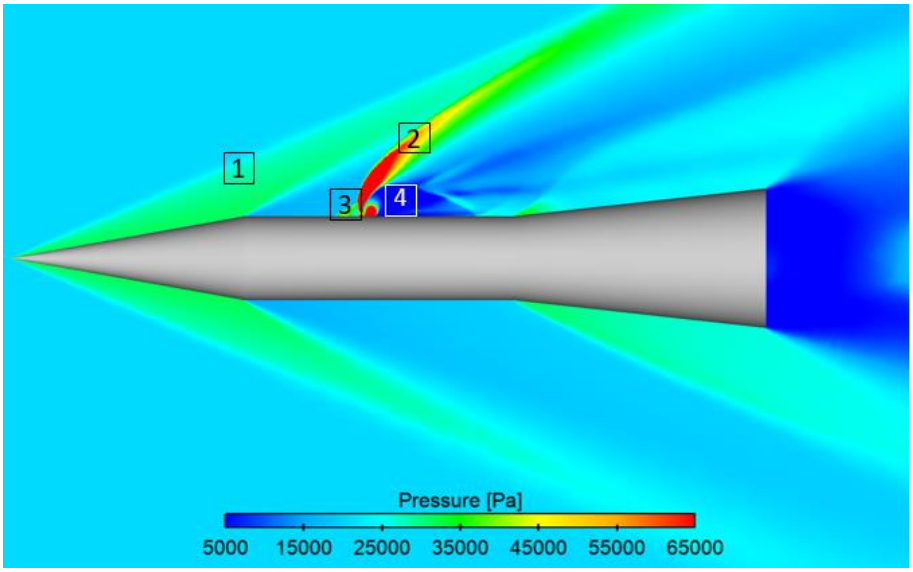

Figure 6: Pressure distribution at the symmetry plane

DOI: 10.13009/EUCASS2022-7236

Mach number distribution obtained from numerical simulation is presented in Figure 7. In addition, a Schlieren image obtained from another lateral jet experiment is presented in Figure 8 [4].

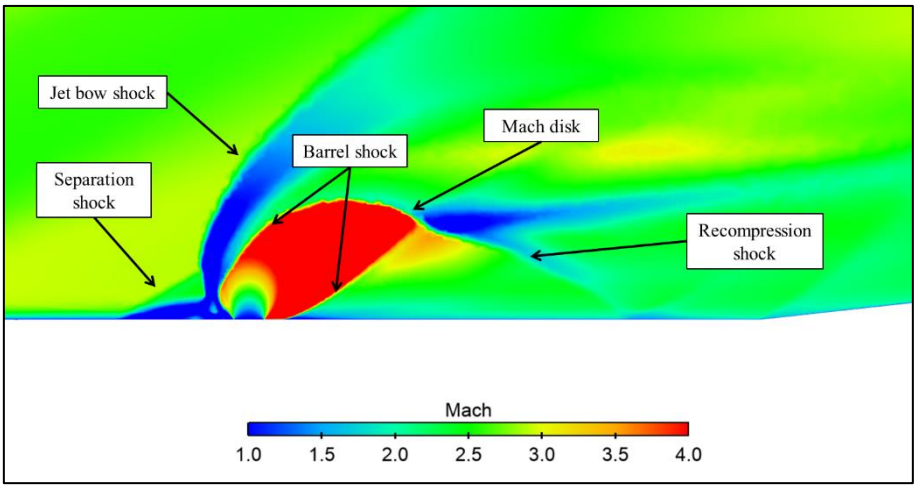

Figure 7: Mach number distribution at the symmetry plane

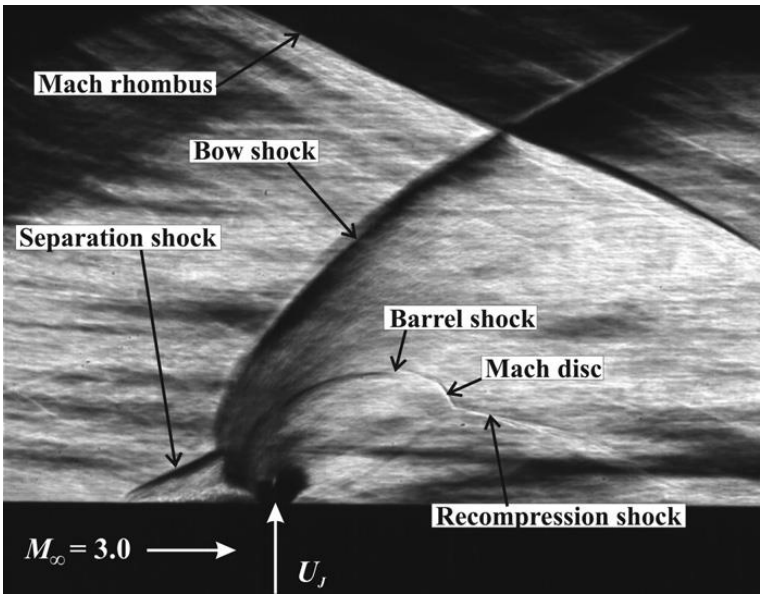

Figure 8: Schlieren image around jet

After comparing the Figure 7 and Figure 8, one can say that results from CFD and experiment are similar. Separation shock which occurs due to the high adverse pressure in the jet vicinity is visible from both figures. Moreover, jet bow shock which occurs due to the interaction of the jet plume obstacle and supersonic freestream can be observed from both figures. Due to under-expanded jet flow, plume is wrapped with barrel shock and Mach disk phenomenon finalizes this region, and both occurrences can be visible from the figures. Recompression shock that stands behind the jet location can be observed from both figures [4]. From the resemblance of the figures one can say that, numerical solution is well enough to capture all flow features in the vicinity of the jet.

3. Lateral jet operating with non-reacting gas mixture

In this test case, a lateral jet on a generic missile model is investigated with a mixture of non-reacting gases. With this investigation, the mixture and interaction of multi-species gases with supersonic crossflow is studied and compared to the experimental results.

DOI: 10.13009/EUCASS2022-7236

3.1 Test case details

The generic missile model with the lateral jet system is modelled for the study [5]. The generic missile has the same geometrical parameters as in Section 2.1 except for a missile diameter (D) of 90 mm and a nozzle geometry representing the end of the lateral jet system. The lateral jet nozzle exit has a diameter of 0.051D (4.6 mm). Also, the lateral jet nozzle has a conical shape which is positioned inside the cylindrical part of the missile and it is assumed that the gas mixture is stored in tank at the start of the nozzle. Mentioned lateral jet nozzle is modelled utilizing the images obtained from the literature [6]. Modelled nozzle geometry is shown in Figure 9.

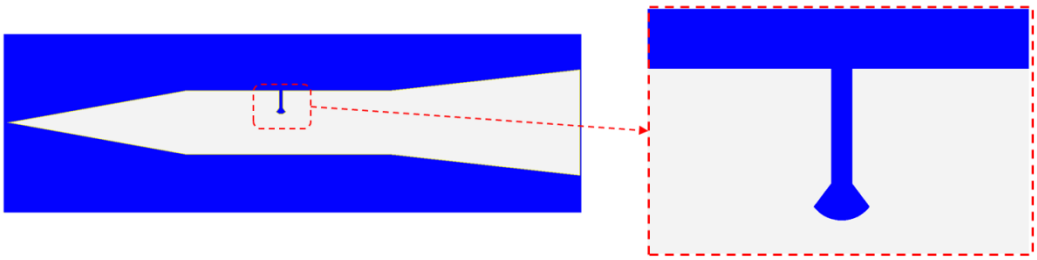

Figure 9: Nozzle geometry of the test case

The reference experimental flow conditions of the supersonic free-stream and the lateral jet flows are given in Table 2 and the gas mixture species and proportions are given in Table 3. In the numerical simulation, copper and lead species which exist in a very limited amount are omitted as in the reference study [5].

Table 2: Flow properties

Crossflow Mach	3
Crossflow Static Temperature (T_∞) [K]	104.6
Crossflow Static Pressure (P_∞) [Pa]	54500
Jet Total Temperature ($T_{0,j}$) [K]	2300
Jet Total Pressure ($P_{0,j}$) [Pa]	12×10^6
Pressure Ratio (PR) – ($P_{0,j}$ / P_∞)	220

Table 3: Jet Species Proportions

Jet Species	**Species Percentage (%)**
CO_2	38.21
H_2	1.73
H_20	10.47
CO	35.47
N_2	14.12

In the reference experiment, static pressure values are measured along the missile at different circumferential angles and radially. Measured pressure values are compared to the numerical analysis results in the next section.

3.2 CFD methodology

Numerical analyses are carried out with the commercial Metacomp CFD++ solver and in the analyses, 2 equation k-ω-SST turbulence model is utilized. In the CFD analyses, “Characteristics based inflow/outflow” boundary condition is used in the free stream flow boundaries, “Inflow-Stagnation Pressure and Temperature” inflow boundary condition is used at the nozzle start which can be defined with characteristic flow conditions and “Wall” boundary condition is used for the remaining surfaces with adiabatic and no-slip condition properties. Mentioned boundary conditions are shown in Figure 10. The chemical reactions that can occur between the species of the gas mixture are not modelled in this study so the secondary combustion is not allowed.

DOI: 10.13009/EUCASS2022-7236

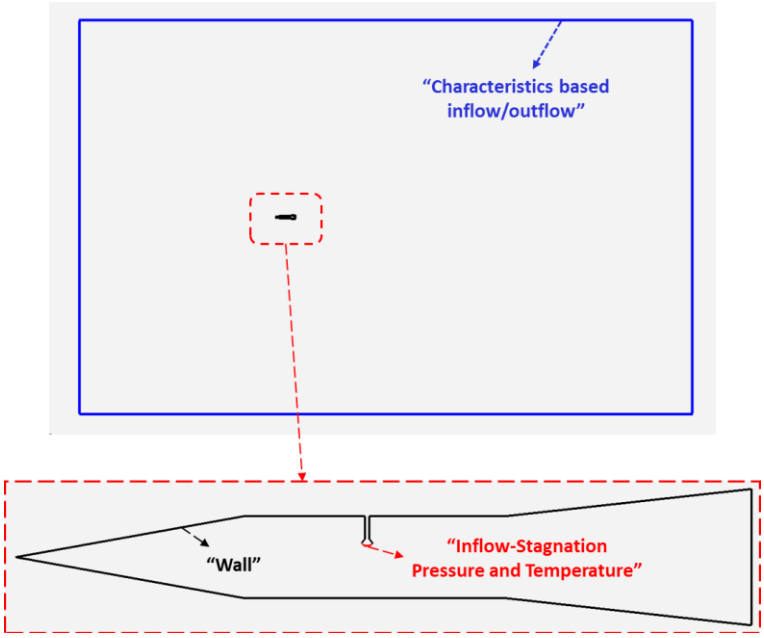

Figure 10: Boundary conditions of the numerical simulation

3.3 Results and discussion

At the end of the numerical analyses, pressure values are obtained at the axial locations at different radial angles and radially at the nozzle axial position. Pressure comparisons are evaluated with the pressure coefficient change.

$$\Delta C_p = C_p - C_{p,no-jet} \quad \textbf{(1)}$$

$C_{p,no\text{-}jet}$ values are obtained with an analysis that the "Inflow-Stagnation Pressure and Temperature" boundary condition is changed with the "Wall" boundary condition at the nozzle entrance surface. The comparisons are carried out for radial lines of 180°, 150° and 120° at the cylindrical part of the missile in terms of X/D lengths. Also at the circumferential line and the nozzle axial position (X/D=4.3) comparisons are made. The comparison is also done with the CFD results carried out with different solvers (ARL and TAU Codes) produced in the reference literature essay [5]. Comparisons are shown in Figure 11, Figure 12, Figure 13 and Figure 14.

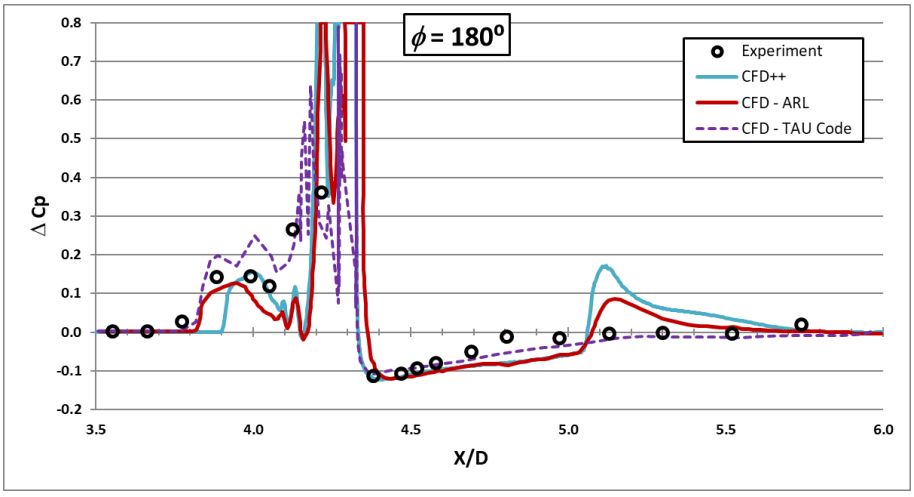

Figure 11: Pressure coefficient differences for 180° circumferential position

DOI: 10.13009/EUCASS2022-7236

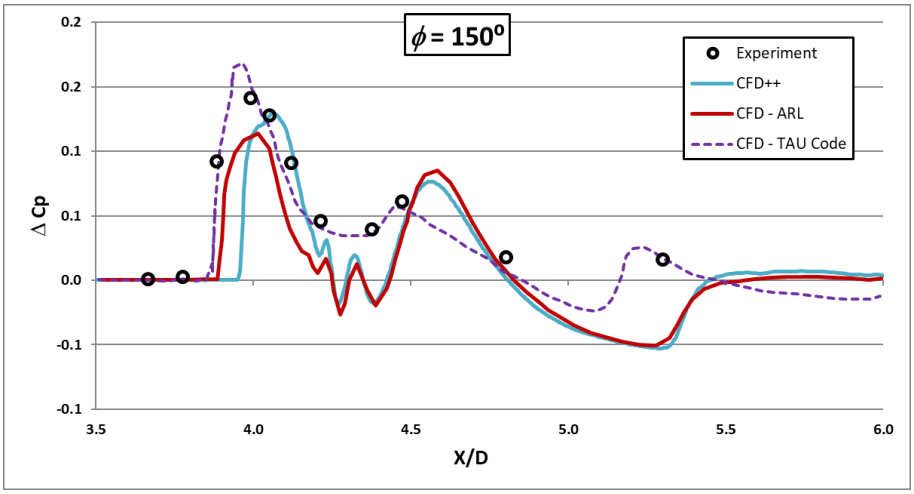

Figure 12: Pressure coefficient differences for 150° circumferential position

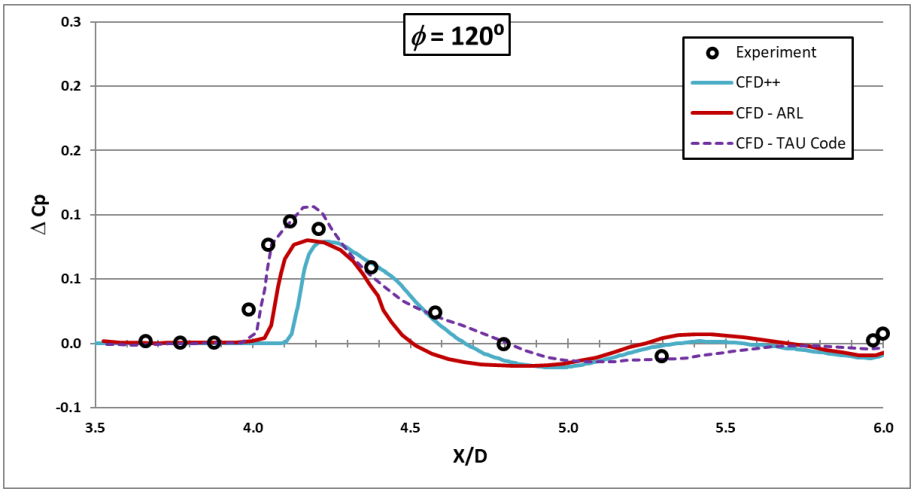

Figure 13: Pressure coefficient differences for 120° circumferential position

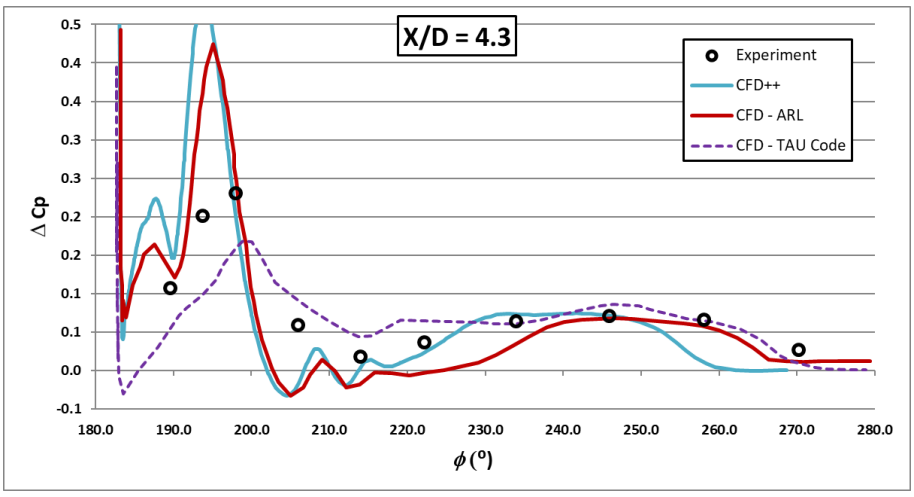

Figure 14: Pressure coefficient differences for X/D = 4.3 axial position

The investigation of pressure coefficient comparisons reveal that the CFD++ results are in better agreement with the experimental results for the 180° axial line and the circumferential line at jet exit (X/D=4.3) than the other comparisons made for 150° and 120° axial lines. Also, the literature CFD study carried out with the TAU Code

DOI: 10.13009/EUCASS2022-7236

solver has better agreement overall except for the circumferential line results. It is evaluated that the difference of the pressure coefficient results is caused by the nozzle geometry modelled with the help of the images from the literature studies and also the omitted secondary combustion mechanism mentioned in Section 3.2. Considering the deductions made, another study is carried out with the secondary combustion allowed which is presented in Section 4.

4. Lateral jet operating with reacting gas mixture

In this test case, upon investigating a non-reacting gas interaction problem, lateral jet – free stream flow aerodynamic interaction is modelled with reaction mechanisms allowed. Investigation of this method is done by comparing the results to the experimental results.

4.1 Test case details

This test case has the same generic missile model mentioned in Section 3.1 except that the nozzle details are not modelled. The nozzle exit has a diameter (D) of 0.051D (4.6 mm) and modelled as a circular plane as a continuation of the cylindrical body since the exact geometrical details of the nozzle is not present in the literature [7]. The reference experimental flow conditions [7] of the supersonic free-stream and the lateral jet flows are given in Table 4 and the gas mixture species and proportions are given in Table 5.

Table 4: Flow properties

Crossflow	**Jet flow**
$M_\infty = 3$	$P_{0,jet}$ [Pa] = 12×10^6
P_∞ [Pa] = 92300	$T_{0,jet}$ [K] = 2300
T_∞ [K] = 105	

Table 5: Gas mixture species and proportions

Free-stream species		**Jet species**	
O_2	% 21	CO_2	% 38.21
N_2	% 79	H_2	% 1.73
		H_2O	% 10.47
		CO	% 35.47
		N_2	% 14.12

The reactions that take place with the mixture of the free-stream flow and the jet gases are given in Eqn. 2, Eqn. 3 and Eqn. 4 which are modelled with numerical simulations.

$$CO + O + M \rightarrow CO_2 + M \quad \textbf{(2)}$$

$$CO + O_2 \rightarrow CO_2 + O \quad \textbf{(3)}$$

$$O_2 + M \rightarrow O + O + M \quad \textbf{(4)}$$

4.2 CFD methodology

Numerical analyses are carried out with the commercial Metacomp CFD++ solver. In the CFD analyses, the same boundary conditions are applied as mentioned in the Section 3.2 except for the jet species and reaction models. Since the reaction models used in the reference study [7] is not specified, several reaction models based on the experimental studies are investigated based on research groups like GRI-Mech 3.0 [8] and San Diego [9]. In the next step, grid independency study is conducted with unstructured meshing methodology. Figures for the different cell number grids are presented in the Figure 15.

DOI: 10.13009/EUCASS2022-7236

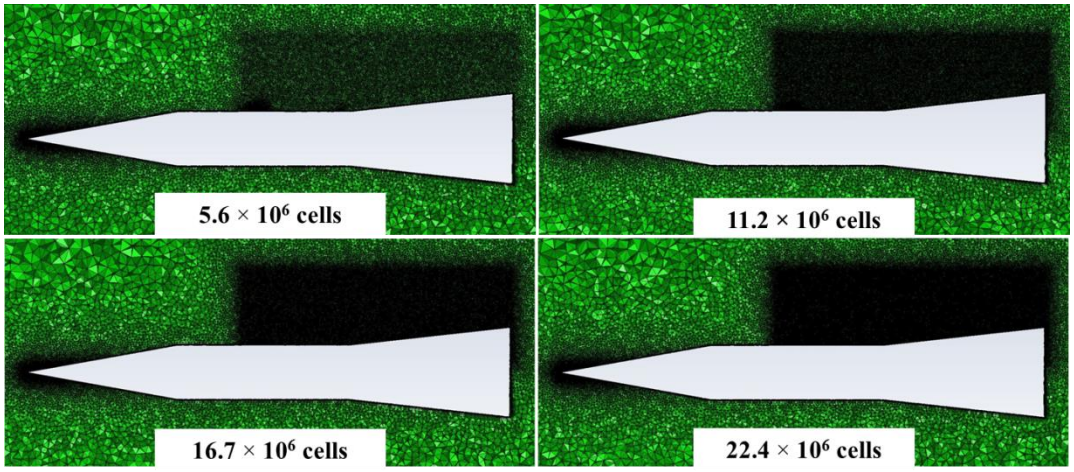

Figure 15: Generated volume grids

Normal force and pitching moment coefficient results for different number of grids are presented graphically in Figure 16 and numerically in Table 6.

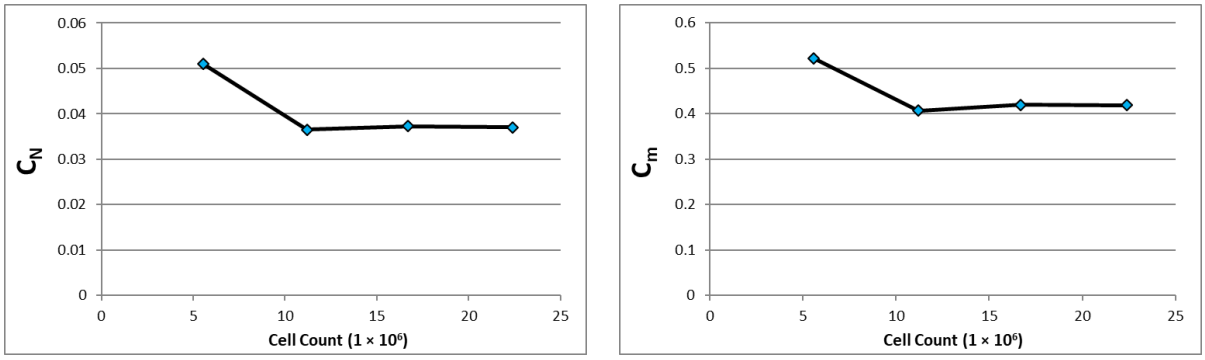

Figure 16: Grid independency results

Table 6: Difference of force and moment coefficients for grids

Cell count (1×10^6)	ΔC_N(%)	ΔC_m(%)
5.55	37.4	24.9
11.2	-1.5	-2.8
16.7	0.6	0.3
22.4		

Investigation for the results of the grid independency study shows that, coefficient differences of the grid with 16.7 million cells from the finest grid are less than 1 percent. As a result of this, it is decided that the grid with the 16.7 million cells is to be used for the rest of study.

4.3 Results and discussion

The mentioned reaction models mentioned in Section 4.2 are studied with the two cost effective 2 equation turbulence models, k-ε Realizable and k-ω-SST. The results of this investigation are presented for the 180° circumferential angle in Figure 17 and Figure 18.

DOI: 10.13009/EUCASS2022-7236

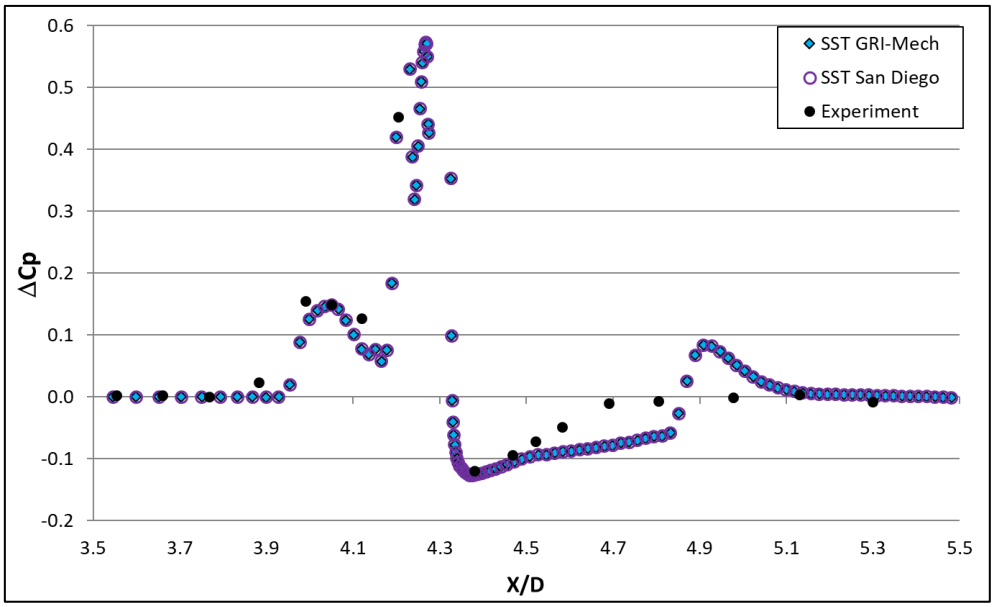

Figure 17: Pressure coefficient differences for two reaction models (k-ω-SST)

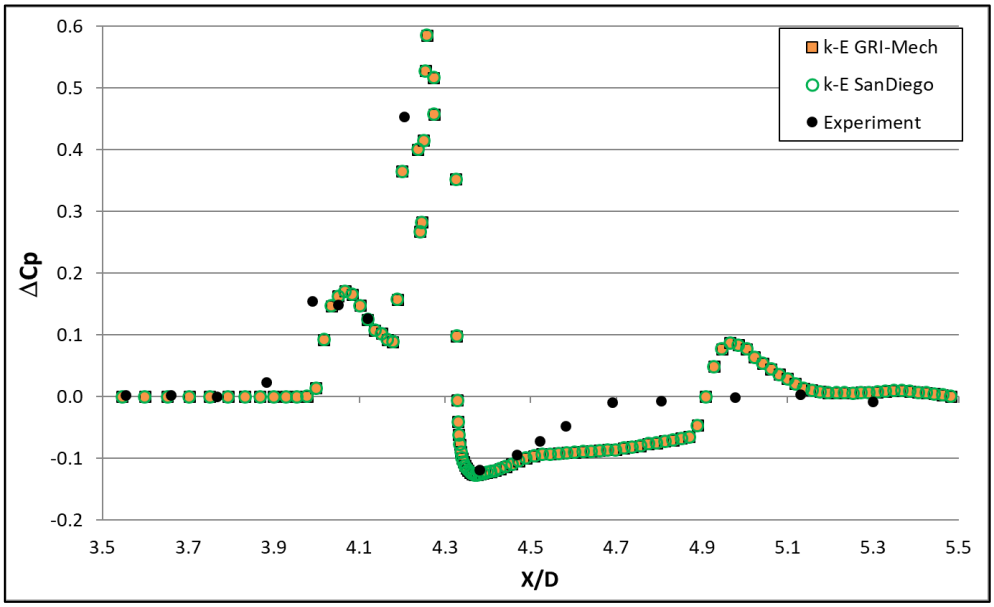

Figure 18: Pressure coefficient differences for two reaction models (k-ε Realizable)

The investigation of reaction models for the same turbulence model showed similar results in terms of the pressure coefficient differences therefore the case can be assumed reaction model independent. With this result in mind, the GRI-Mech reaction model is used for the turbulence model selection study. With the k-ω-SST model having better agreement with the experimental results (Figure 19), it is compared to the 1-equation Spalart –Allmaras model and 7-equation "2nd moment closure" models present in the CFD++ solver. The comparison is presented for the 180° circumferential angle in Figure 20 with the numerical results from the literature study [7] added.

DOI: 10.13009/EUCASS2022-7236

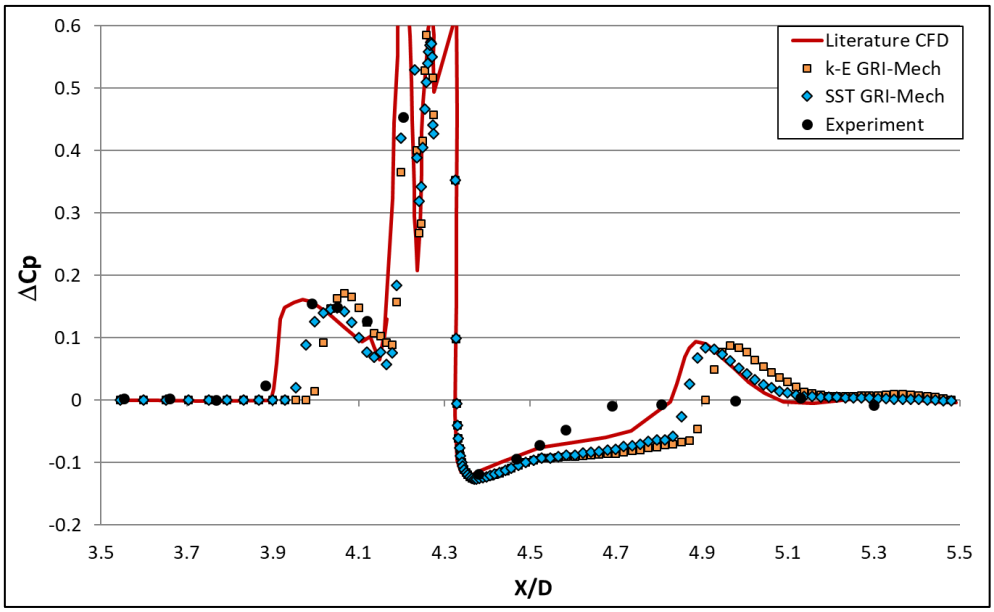

Figure 19: Pressure coefficient differences for two turbulence models - I

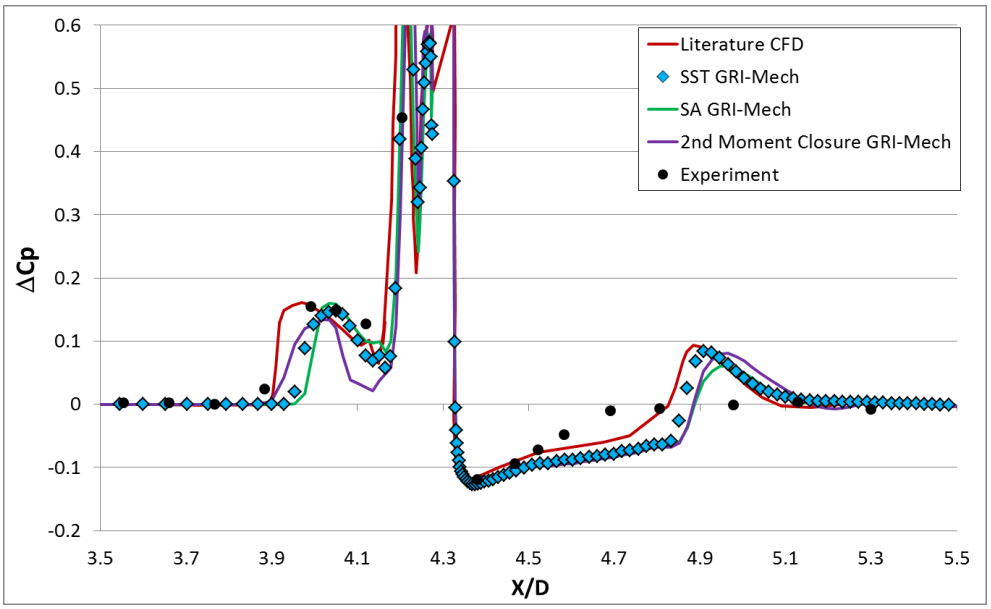

Figure 20: Pressure coefficient differences for several turbulence models - II

The results given in Figure 19 and Figure 20 show that k-ω-SST turbulence model gives the best results compared to the other ones. The pressure coefficient difference results show that including secondary combustion effects in the numerical simulation improves results which can be seen by comparing the non-reacting results given in Figure 11 and the reacting results given in Figure 20. The pressure coefficient differences at the separation shock region ($3.9<X/D<4.2$) and the reattachment region ($4.8<X/D<5.1$) are in a better agreement than the non-reacting results. Also there seems to be no improvement for the pressure coefficient differences at the pressure recovery region ($4.4<X/D<4.8$).

After the numerical comparison, Mach number distribution comparison is presented in Figure 21 for a further investigation of the flow phenomenon.

DOI: 10.13009/EUCASS2022-7236

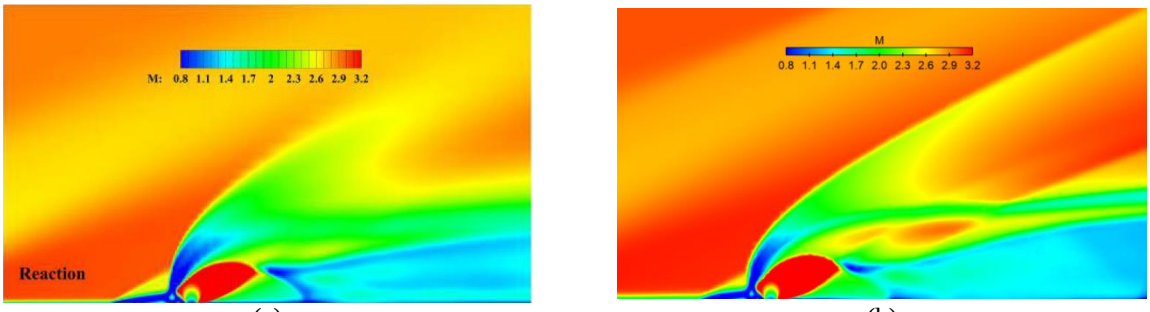

(a) (b)

Figure 21: Flow field Mach number distribution comparison (a: literature results, b: study results)

Investigation of Mach distributions reveals that similar flow phenomena like separation shock, jet bow shock, barrel shock and Mach disk can be observed from both results. Output of the both analyses indicates that similar shock formations occur near the jet exit due to interactions. However, the CFD tools produce different flow formations at the reattachment region, recirculation region and the region beyond the Mach disk. It can be said that the differences between both the numerical results and the experimental results arise from lack of capturing the phenomena behind the jet accurately.

5. Conclusion

In the study, aerodynamic investigation of lateral jet systems which overcome the problems with the conventional control systems are carried out. Investigation on this case in the aspect of jet and crossflow interaction is accomplished by using the commercially available computational fluid dynamics software. The selection of numerical simulation methods for solving lateral jet in supersonic crossflow is handled by applying several approaches on three different test cases with experimental results.

First of the numerical simulation methods is applied for an air spouting lateral jet for the validation purposes. Comparison between numerical and experimental results is made using the surface pressure data and Schlieren image photography. Other two studies compose of jets which are operating with combustion products. In the second study, multi-species jet flow and crossflow interactions are examined without reaction mechanisms. In the last study, the effects of secondary combustion of the jet flow gases are included in the numerical simulation using two different reaction models. Results are presented using the surface pressure and Mach number distributions in the flow field.

The first study results show that, for cases with single species gas interaction, the prediction of the flow field and the surface pressure is successful. Surface pressure results show that the effect of the jet flow diminishes as marching away from jet exit in the circumferential direction as expected. Also the investigation of flow field Mach number distribution shows that the expected flow formations are present when compared to a Schlieren image from an example lateral jet experiment. The results of the second study with the non-reacting multi-species flow mixture is not as good as the single-species study since the pressure coefficient starts to differentiate especially at the separation shock and reattachment shock regions. The reasons behind the lack of prediction accuracy at these regions are deducted that the available nozzle geometry in the literature lacks details and secondary combustion effects are not included in the numerical simulation. In the last study with the reacting multi-species flow mixtures, several alternatives regarding simulation method are implemented with turbulence model and reaction model studies. Upon completing a grid convergence study, k-ε Realizable and k-ω-SST turbulence models are utilized with GRI-Mech and San Diego reaction models. This utilization reveals that the case is reaction model independent for these models and GRI-Mech model is used for the final method investigation. With this, the turbulence model investigation is expanded with 1-equation Spalart-Allmaras model and 7-equation 2nd moment disclosure models resulting with the k-ω-SST model achieving best results. The final investigation is carried out with the determined grid, GRI-Mech reaction model and k-ω-SST turbulence model. Examination of the results indicates that (compared to the non-reacting study) including the reaction mechanisms in the numerical simulation improved the surface pressure distribution in several locations such as separation-reattachment regions excluding the wake region. Compared to the experimental results, the literature CFD simulation is in better agreement at the separation region and slightly better at the start of the wake region. It is inferred that, to be able to obtain closer results to the experimental data, this study can be extended by utilizing structured grid and more advanced turbulence models.

DOI: 10.13009/EUCASS2022-7236

The investigation of several test cases reveals that, utilized CFD methodology is sufficient for modelling the lateral jet in supersonic crossflow in general aspects. However, multi-species mixture problems require out of ordinary approaches for better prediction of flow pattern even when reaction mechanisms are allowed. Mentioned approaches consist of applying methods such as hybrid RANS/LES and LES or specialized commercial methods like GEKO (available in Ansys Fluent [10]) and using non-linear turbulence models like cubic k-ε and Hellsten (available in Metacomp CFD++ [11]). Also, extending this study with the use of the structured grids and different reaction models may be beneficial.

Acknowledgement

Authors would like to thank Roketsan Missiles Inc. and Aerodynamic and Engineering Analysis Department for supporting this study.

References

[1] Gnemmi, P., R. Adeli, and J. Longo. 2008. Computational Comparisons of the Interaction of a Lateral Jet on a Supersonic Generic Missile. In: *AIAA Atmospheric Flight Mechanics Conference and Exhibit*. *https://doi.org/doi:10.2514/6.2008-6883.*

[2] Dağlı, E. C., and M. H. Aksel. 2018. Numerical Simulation of Lateral Jet in a Supersonic Missile Using Computational Fluid Dynamics. In: *18th International Conference on Machine Design and Production (UMTIK 2018).* 457–468.

[3] Dağlı, E. C. 2019. Numerical Simulation of Lateral Jets in Supersonic Crossflow of Missiles using Computational Fluid Dynamics. MSc Thesis. Middle East Technical University.

[4] Stahl, B., H. Emunds, and A. Gülhan. 2009. Experimental Investigation of Hot and Cold Side Jet Interaction with a Supersonic Cross-flow. *Aerospace Science and Technology*. *13*(8):488–496. *https://doi.org/10.1016/J.AST.2009.08.002*.

[5] DeSpirito, J. 2015. Effects of Turbulence Model on Prediction of Hot-Gas Lateral Jet Interaction in Supersonic Crossflow. In: *53rd AIAA Aerospace Sciences Meeting*.

[6] Höld, R. K., M. Engert, K. Weinand, and D. Stern. 2010. Numerical Investigation of Hot and Cold Side Jet Interaction with a Supersonic Cross-Flow, *New Results in Numerical and Experimental Fluid Mechanics VIII.* 558–582.

[7] Dong, H., J. Liu, Z. Chen, and F. Zhang. 2018. Numerical Investigation of Lateral Jet with Supersonic Reacting Flow. *Journal of Spacecraft and Rockets.* Vol. 55(4). 928–935.

[8] Smith, G. P., D. M. Golden, M. Frenklach, N. W. Moriarty, B. Eiteneer, M. Goldenberg, C. T. Bowman, R. K. S. Song, W. C. Gardiner Jr., V. V. Lissianski, and Z. Qin. GRI-Mech 3.0. https://www.combustion.berkeley.edu/gri-mech/ (accessed Feb. 11, 2020).

[9] Mechanical and Aerospace Engineering (Combustion Research) University of California at San Diego, Chemical-Kinetic Mechanisms for Combustion Applications. The San Diego Mechanism. https://www.web.eng.ucsd.edu/mae/groups/combustion/mechanism.html (accessed Feb. 11, 2020).

[10] Ansys Inc., Ansys Fluent 2021 R1 – Theory Guide, 2021.

[11] Metacomp Technologies Inc., CFD++ Version 20.1 – User Manual, 2021.